Rapid Communications | Editors' Suggestion

Semiconducting cubic titanium nitride in the Th_3P_4 structure

Venkata S. Bhadram,[1,*] Hanyu Liu,[1] Enshi Xu,[2] Tianshu Li,[2] Vitali B. Prakapenka,[3] Rostislav Hrubiak,[4] Stephan Lany,[5] and Timothy A. Strobel[1,†]

[1]*Geophysical Laboratory, Carnegie Institution for Science, 5251 Broad Branch Road, Washington, D.C. 20015, USA*

[2]*Department of Civil and Environmental Engineering, George Washington University, Washington, D.C. 20052, USA*

[3]*Center for Advanced Radiation Sources, The University of Chicago, 5640 South Ellis Avenue, Chicago, Illinois 60637, USA*

[4]*High Pressure Collaborative Access Team (HPCAT), Geophysical Laboratory, Carnegie Institution of Washington, Argonne, Illinois 60439, USA*

[5]*National Renewable Energy Laboratory, Golden, Colorado 80401, USA*

(Received 3 October 2017; published 22 January 2018)

We report the discovery of a long-sought-after phase of titanium nitride with stoichiometry Ti_3N_4 using diamond anvil cell experiments combined with *in situ* high-resolution x-ray diffraction and Raman spectroscopy techniques, supported by *ab initio* calculations. Ti_3N_4 crystallizes in the cubic Th_3P_4 structure [space group $I\bar{4}3d$ (220)] from a mixture of TiN and N_2 above ≈75 GPa and ≈2400 K. The density (≈5.22 g/cc) and bulk modulus ($K_0 = 290$ GPa) of cubic-Ti_3N_4 (c-Ti_3N_4) at 1 atm, estimated from the pressure-volume equation of state, are comparable to rocksalt TiN. *Ab initio* calculations based on the *GW* approximation and using hybrid functionals indicate that c-Ti_3N_4 is a semiconductor with a direct band gap between 0.8 and 0.9 eV, which is larger than the previously predicted values. The c-Ti_3N_4 phase is not recoverable to ambient pressure due to dynamic instabilities, but recovery of Ti_3N_4 in the defect rocksalt (or related) structure may be feasible.

DOI: 10.1103/PhysRevMaterials.2.011602

Mononitrides (MN) of group 4 elements (M = Ti, Zr, and Hf) with the rocksalt (rs) NaCl structure are known for their extraordinary hardness, high melting points, and chemical inertness. They are commonly used as coatings on cutting tools for wear protection. These nitrides are metallic due to the presence of a residual electron per atom in the metal d orbital and therefore possess a large density of states at the Fermi level. The metallic nature of these compounds finds applications in microelectronic industries, and the inherent low-temperature superconducting properties exhibited by these compounds are of fundamental interest [1–3].

On the other hand, the nitrogen-rich nitrides of group 4 elements with 3:4 stoichiometries (M_3N_4, M = Ti, Zr, and Hf) are not as common compared to their group 14 counterparts (A_3N_4, A = Si, Ge, and Sn) [4–8]. Unlike 3:4 nitrides of group 14 elements which exhibit trigonal $P31c$ (α), hexagonal $P6_3/m$ (β), and cubic $Fd\bar{3}m$ (γ) modifications [6], the stoichiometric 3:4 nitrides of group 4 elements were initially only known to exhibit orthorhombic $Pna2_1/Pnam$ structures [9–11]. Zerr *et al.* [12] have synthesized cubic phases of Zr_3N_4 and Hf_3N_4 (c-Zr_3N_4 and c-Hf_3N_4) with the Th_3P_4-type structure (space group $I\bar{4}3d$) using the laser-heated diamond anvil cell (LH-DAC) technique at pressures of 16 and 18 GPa, respectively. The structural solutions reported by Zerr *et al.* [12] were strongly supported by the theoretical predictions of Kroll [13]. Later, synthesis of bulk powders of c-Zr_3N_4 using the multianvil apparatus [14], and deposition of c-Zr_3N_4 thin films using an industrially viable, modified filtered cathodic arc method were reported [15]. The extraordinary wear resistance of this cubic phase was demonstrated using milling tests on carbide tools that were coated with c-Zr_3N_4 films [15]. More interest in these cubic nitrides pertained to the fact that they are narrow band-gap semiconductors with relatively large dielectric constants and could also exhibit superconductivity with appropriate doping [13,16].

Although much experimental work has been performed on c-Zr_3N_4 and c-Hf_3N_4, the remaining 3:4 nitride in the group 4 trio, i.e., c-Ti_3N_4, has not been realized experimentally. In fact, there were no experimental reports on other theoretically predicted nitrogen-rich titanium nitrides [17,18] until the recent report on LH-DAC synthesis of TiN_2 (titanium pernitride) and the concomitant recovery of this metastable phase to ambient conditions [19]. The high N_2 chemical potential (0.6 eV/N) required to stabilize the c-Ti_3N_4 phase is not achievable in the conventional ammonolysis method [20]. Kroll [13] predicted that c-Ti_3N_4 would be accessible at about 100 GPa. Previous experimental efforts by Zerr *et al.* [12] were unsuccessful in forming c-Ti_3N_4, possibly due to the low synthesis pressures (25 GPa) used in their experiments. Given the enormous recent interest in metastable group 4 nitrides [20,21], solid solutions [22], and two-dimensional (2D) forms [23], the experimental realization of c-Ti_3N_4 is of great importance.

In this Rapid Communication, we report the synthesis of c-Ti_3N_4 at a pressure of ≈75 GPa using the LH-DAC technique with *in situ* characterization using x-ray diffraction (XRD) [24] and Raman spectroscopy. Our experimental results corroborate the theoretical calculations including structure searching using the swarm intelligence-based CALYPSO code [25,26], and first-principles density functional theory (DFT) calculations within the Perdew-Burke-Ernzerhof (PBE) [27] parametrization of

*vbhadram@carnegiescience.edu
†tstrobel@carnegiescience.edu

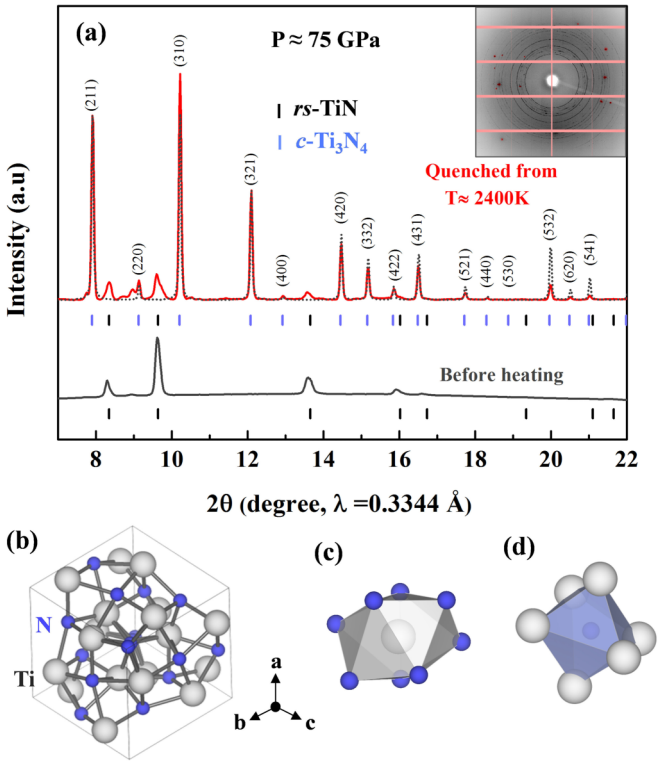

FIG. 1. (a) Synchrotron XRD pattern of TiN + N_2 mixture before and after laser heating inside the DAC. The inset shows the corresponding diffraction rings on the 2D image plate after laser heating. The tick marks indicate the Bragg peaks from c-Ti_3N_4 and rs-TiN phases. The black dotted curve represents the calculated pattern of c-Ti_3N_4. (b) Ball-and-stick model of c-Ti_3N_4. The coordination polyhedron of (c) Ti and (d) N.

the generalized gradient approximation (GGA). We have also employed the G_0W_0 level approximation, as well as the Heyd-Scuseria-Ernzerhof (HSE06) [28] hybrid functional, for more accurate estimations of the band gap. The detailed description of the experimental and theoretical methods can be found in the Supplemental Material [29].

The synthesis conditions for c-Ti_3N_4 are similar to those that were used previously for TiN_2 [19]. A compressed TiN powder platelet ($\sim 50 \times 50 \times 10\ \mu m^3$) was loaded in the sample chamber of the DAC. The chamber was then filled with dense nitrogen gas (pressure medium), compressed to 75 GPa, and heated in temperature steps until a reaction was observed. While heating the sample, XRD data were collected from the flattop laser-heated spot on the sample at each temperature step. Upon heating to $T > 2400$ K, diffraction rings other than those from rs-TiN and N_2 were observed on the 2D image plate [Fig. 1(a)]. These new sharp and well-resolved diffraction rings were easily distinguishable from TiN and N_2 (the intensities of which reduced significantly) due to the phases having different textures [the inset of Fig. 1(a)]. All of the new Bragg peaks were indexed to an I-centered cubic lattice using CRYSFIRE and CHECKCELL [30] programs. The obtained lattice parameter from the Le Bail refinement of the XRD pattern was $a = 5.946(1)$ Å (see Fig. S1 [29]). A crystal structure search performed at 70 GPa resulted in c-Ti_3N_4 with the Th_3P_4-type structure (space group $I\bar{4}3d$, $Z = 4$) and the structural optimization using DFT gave the atomic positions for Ti (0.375, 0.000, 0.250) and N(0.076 36,0.076 36,0.076 36). Although at different pressures, our structural solution is in agreement with the previous report [13]. As shown in Fig. 1(a), the calculated diffraction pattern is in excellent agreement with the observed one. The detailed descriptions on the various aspects of the Th_3P_4-type structure are given elsewhere [31]. In c-Ti_3N_4, Ti is surrounded by eight N atoms with bisdisphenoidal coordination (dodecahedral). N is coordinated by six Ti atoms forming a distorted octahedron [as shown in Figs. 1(b)–1(d)]. The coordination number of Ti in Ti_3N_4 is higher than the corresponding mononitrides with the rocksalt structure.

As presented previously [19], when TiN_2 was synthesized by reacting TiN with N_2 at $P \approx 73$ GPa and $T > 2300$ K, additional Bragg peaks were observed that could not be described by TiN, TiN_2, and any of the known phases of N_2. Reanalysis of the previously unidentified Bragg peaks gives an excellent match with the c-Ti_3N_4 phase (see Fig. S2 [29]), indicating that c-Ti_3N_4 and TiN_2 may coexist depending on the bulk TiN + N_2 composition (it is to be noted that we did not observe the formation of TiN_2 in experiments with low bulk N_2 content in the sample chamber, as depicted by the optical micrograph in the inset of Fig. 3). During the decompression process for nitrogen-rich samples, the diffraction from TiN, TiN_2, and c-Ti_3N_4 was present until ≈11 GPa, and at 1 atm only the diffraction from TiN_2 and TiN was observed (see Fig. S1 [29]). Hence, c-Ti_3N_4 and TiN_2 phases may coexist above ≈11 GPa, and, unlike TiN_2, c-Ti_3N_4 is not recoverable at 1 atm. The coexistence of the two phases is consistent from a thermodynamic perspective by the computational convex hull at 70 GPa (see Fig. S3 [29]) and is also suggested by recent calculations by Sun *et al.* [20] based on the nitrogen chemical potential.

The pressure-volume (P-V) relation of c-Ti_3N_4 between 11 and 73 GPa, obtained during decompression, is shown in Fig. 2(a). Due to a large pressure step during decompression, the exact pressure at which c-Ti_3N_4 becomes unstable was not determined; however, the instability occurs somewhere between 11 GPa and 1 atm (see Fig. S2 [29]; it is around 5 GPa as per the Raman data below). The P-V data were fitted with a third-order Birch-Murnaghan equation of state (EOS) and the obtained volume at 1 atm is $V_0 = 62.5 \pm 0.2$ Å^3/f.u. and the isothermal bulk modulus $K_0 = 290 \pm 11$ GPa (with $K_0' = 3.5 \pm 0.6$). The bulk modulus of c-Ti_3N_4 is similar to TiN ($K_0 = 294$ GPa) and is much less than that of TiN_2 ($360 < K_0 < 385$ GPa) [19]. The estimated density of c-Ti_3N_4 at 1 atm is 5.22 g/cc, which is slightly smaller than that of TiN (5.4 g/cc).

The thermodynamic behavior of c-Ti_3N_4 was investigated further via DFT calculations using different functionals for the exchange correlation energy [PBEsol and local density approximation (LDA)]. The lattice volumes obtained using PBEsol showed very good agreement with experiment with an average absolute deviation of 0.017 Å^3/f.u. in volume over the entire pressure range, whereas LDA consistently underestimates volume for a given pressure. The formation enthalpy of c-Ti_3N_4 is positive below 36 GPa, and at 1 atm the phase is

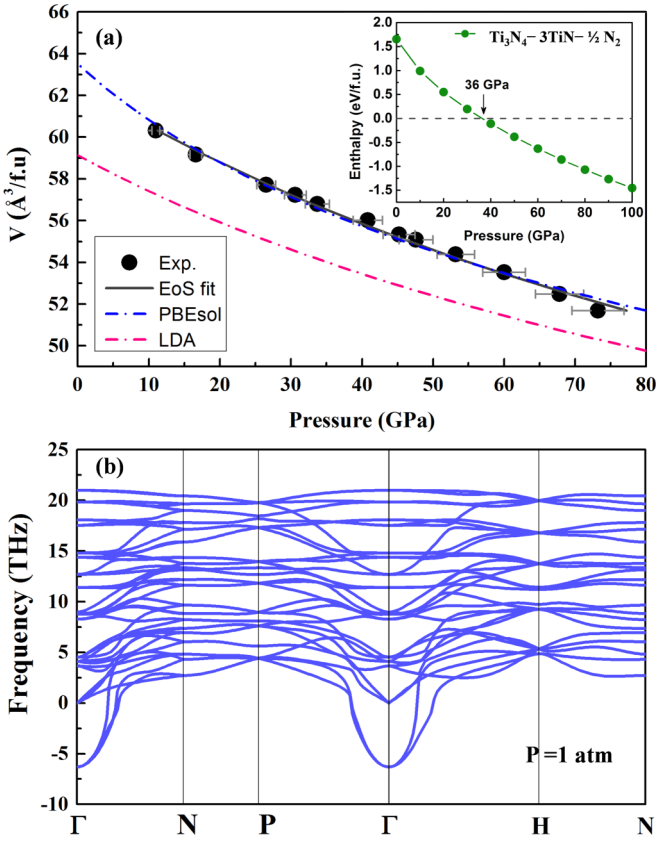

FIG. 2. (a) *P*-*V* data for *c*-Ti_3N_4. The colored dashed-dotted lines represent the calculated *P*-*V* relations using different functionals. The estimated standard deviations (e.s.d.) in experimental volume are much smaller than the size of the data symbols (black circles). The inset shows the thermodynamic stability at 0 K of *c*-Ti_3N_4 as a function of pressure (calculated using the PBE functional). (b) Calculated phonon dispersion of *c*-Ti_3N_4 at ambient pressure (1 atm). Phonon dispersion at 70 GPa is shown in Fig. S4 [29].

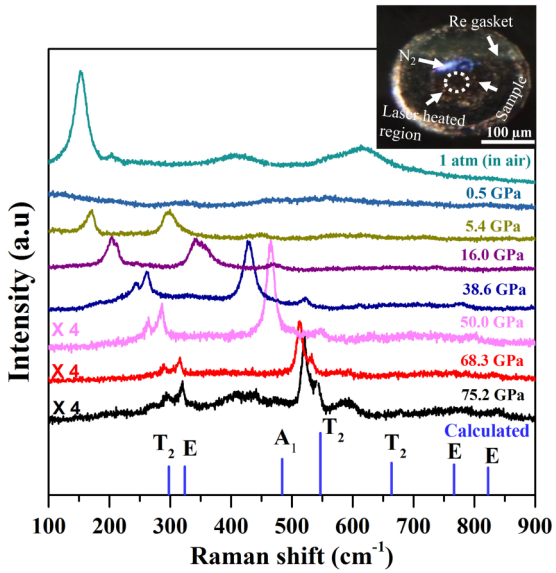

FIG. 3. Raman spectra of *c*-Ti_3N_4 collected from the laser-heated spot on the sample during decompression run. All the Raman modes at 1 atm match with that of TiO_2 (anatase/rutile), indicating the oxidation of the sample after the Raman measurement in air. The solid vertical lines represent the calculated Raman modes of *c*-Ti_3N_4 at 70 GPa. The inset shows the optical micrograph of the sample chamber inside the DAC.

metastable by 1.66 eV/f.u. with respect to disproportionation into TiN + N_2 [see the inset of Fig. 2(a)]. As shown in Fig. 2(b), the calculated phonon dispersion relations of *c*-Ti_3N_4 at 1 atm showed imaginary frequencies at the zone center indicating dynamic instability of this phase at ambient pressure, despite the fact that the elastic constants for this phase are all positive [16]. Further, we have constructed convex hull diagrams for nitrogen-rich phases in the Ti-N system (see Fig. S3 [29]) that are stable against transformation/decomposition into any other phases. In agreement with our experimental observations, the convex hull diagrams indicate that both Ti_3N_4 and TiN_2 phases are stable at 70 GPa. While TiN_2 becomes stable between 20 and 30 GPa, Ti_3N_4 can be stabilized only above ≈36 GPa. Actual experimental synthesis pressures are higher (≈70 GPa) due to entropic contributions of the gaseous reactant not accounted for in the static calculations [13]. It is to be noted that although the convex hull diagrams in the previous report [18] were able to represent the stability of the TiN_2 phase correctly, *c*-Ti_3N_4 was not predicted, even at a higher pressure of 60 GPa.

The Raman spectra collected from the laser-heated spot on the sample at different pressures during slow decompression is shown in Fig. 3. All the peaks in the Raman spectrum at high pressure can be considered to originate from the *c*-Ti_3N_4 phase, as the residual TiN phase present in the sample (as seen in the XRD pattern) does not have any symmetry-allowed (space group $Fm\bar{3}m$) Raman active modes (see Fig. S5 [29]). According to factor group analysis for the Th_3P_4 structure [32], there are nine Raman active modes for *c*-Ti_3N_4 : $\Gamma_{\text{Raman}} = A_1 + 3E + 5T_2$. We have observed seven modes whose frequencies and intensities match fairly well with the calculated Raman modes of *c*-Ti_3N_4 at 70 GPa (see Fig. 3). The two T_2 modes whose intensities are found to be negligible in our calculations were absent in our measured spectrum. Nevertheless, the features in the Raman spectrum of *c*-Ti_3N_4 were similar to the Raman spectra of its Zr and Hf counterparts with the Th_3P_4 structure [12,15], giving additional confirmation of our reported structure. On decompression, the Raman signal was present until $P \approx 5$ GPa, below which all of the Raman peaks disappeared, indicating the instability of this phase below this pressure. This observation is consistent with the XRD analysis presented above. At ambient conditions, after opening the DAC, the sample was oxidized due to laser irradiation while collecting the Raman spectrum. The oxidation of the sample is clearly seen from the Raman modes, which match both the *rutile* and *anatase* phases of TiO_2 [33,34].

Although *c*-Ti_3N_4 was predicted to be a narrow band-gap semiconductor similar to *c*-Zr_3N_4 and *c*-Hf_3N_4, [13], details of the electronic band structure were missing in the literature. We calculated the band structure of *c*-Ti_3N_4 at 1 atm using the primitive cell of a body-centered-cubic lattice with six Ti and eight N atoms at PBE [27], HSE06 [28], and G_0W_0 (starting wave functions from both PBE and HSE06) levels, as implemented in the VASP package [35,36]. The valence

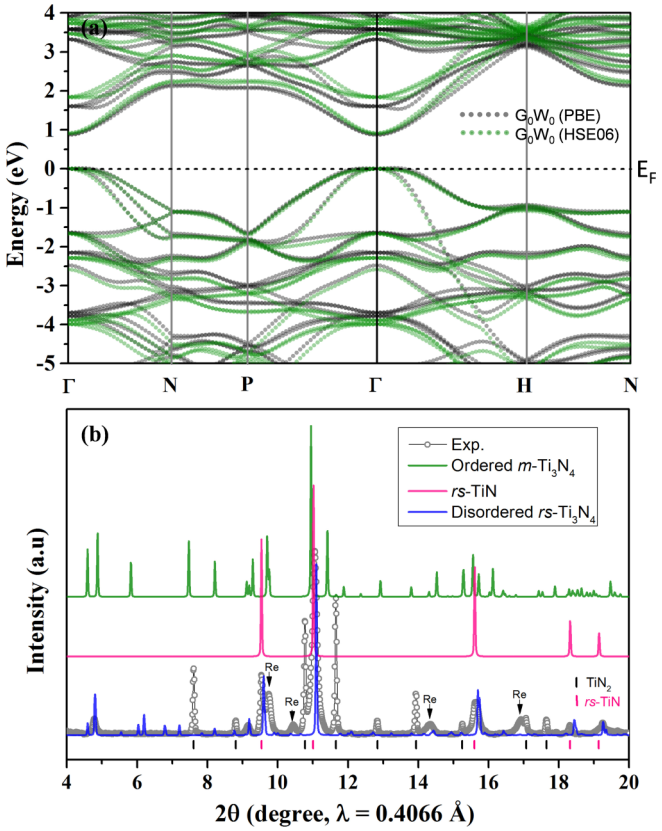

FIG. 4. (a) Band structure of c-Ti_3N_4 around the band edges along the high-symmetry lines of BCC. The selected high-symmetry points in the first Brillouin zone are Γ[0,0,0], N[0.0,0.5,0.0], H[−0.5,0.5,0.5], and P[0.25,0.25,0.25]. The G_0W_0 calculation from the PBE wave function (black dots) reveals a 0.87 eV direct band gap at Γ, while G_0W_0 calculation from the HSE06 wave function (green dots) shows a 0.91 eV band gap. (b) Comparison of experimental XRD pattern (gray circles and line) of the recovered sample at ambient conditions with the corresponding calculated XRD patterns of disordered rs-Ti_3N_4 (blue line), ordered m-Ti_3N_4 (green line), and rs-TiN (pink line) phases.

electrons of Ti include ten electrons from the 3d orbital and four electrons from the 4s and 4p orbitals. All methods show that c-Ti_3N_4 has a direct band gap at the gamma point [Fig. 4(a)]. Among these methods, the PBE calculation yields a small band gap around 0.15 eV, while the hybrid functional HSE06 predicts the gap to be 0.81 eV. The latter is found to be consistent with the quasiparticle predictions based on the G_0W_0 method using different input wave functions, i.e., 0.87 eV with PBE, and 0.91 eV with HSE06. These theoretical predictions thus suggest the actual band gap of c-Ti_3N_4 should be around 0.8–0.9 eV. Since the previous work [13] had also predicted a larger gap of the Zr and Hf counterparts of c-Ti_3N_4 at the PBE level (0.7 and 1.1 eV, respectively), we expect the experimental gaps of $(Zr,Hf)_3N_4$ to be even greater than that of c-Ti_3N_4, in line with the common trend of the G_0W_0 correction relative to PBE. From a structural perspective, we further anticipate that $(Ti,Zr,Hf)_3N_4$ all have smaller band gaps than their corresponding cubic spinel γ-Si_3N_4-type structures because the richness of their valence electrons renders the solids less covalent.

Metal nitrides are well known for their extraordinary range of metastability and can persist at energy scales comparable to 1 eV/atom with respect to their formation elements [20,22,37]. While our calculations showed a dynamical instability for c-Ti_3N_4, the question remains why an ambient-pressure phase of Ti_3N_4 is not recovered, considering, in particular, that other lower-density forms of $(Zr,Hf)_3N_4$, are known [13,38,39]. Our experimental results could be interpreted with the assumption of decomposition into rs-TiN and N_2 below 5 GPa. However, such decomposition is not typically observed in other metastable nitrides. We therefore performed additional structure predictions for possible metastable, ambient-pressure phases of Ti_3N_4. These predictions were performed with a modified version of the kinetically limited minimization approach originally designed for amorphous materials [40]. Appropriate constraints of interatomic distances were implemented to exclude phase-separated structures containing N_2 molecules from the search (see Supplemental Material [29]). We predict a monoclinic, ambient-pressure m-Ti_3N_4 phase [space group $C2/m$ (12)] that can be described as an ordered vacancy compound, constructed from an eight-atom supercell of the two-atom rs-TiN primitive cell with one Ti vacancy. The vacancy arrangement is such that N occurs only in four- and fivefold coordinated configurations, close to the average 4.5 coordination required by stoichiometry. This is a semiconducting phase with a predicted indirect band gap of 0.6 eV. This phase was also predicted to be the most stable form of Ti_3N_4 at 1 atm using the CALYPSO code and is dynamically stable (see Fig. S6 [29]). The simulated XRD pattern of this structure shows additional peaks that were not observed experimentally [see Fig. 4(b)]. One possibility is that, after decompression, c-Ti_3N_4 transforms into a defect rs phase with a disordered vacancy arrangement. For example, we sampled structures with 112 atoms in the primitive cell based on a $4 \times 4 \times 4$ rs supercell, searching for disordered vacancy arrangements that preserve the exclusive four- and fivefold coordination of N using a Monte Carlo approach similar as in the recent work [41]. These structures have a moderate average energy of 55 meV/atom above the ordered m-Ti_3N_4 phase. For comparison, a fully randomly disordered vacancy rs phase lies at 104 meV/atom and the (dynamically unstable) c-Ti_3N_4 phase at 182 meV/atom under ambient pressure. As shown in Fig. 4(b), for a representative disordered structure, the vacancy disorder removes many of the diffraction peaks. Additional disorder over longer length scales is difficult to consider computationally and is likely to further average the diffraction peak intensities towards those of rs-TiN, thus, the two phases would be difficult to distinguish experimentally aside from the most intense features. The most intense non-rs-derived peak near $2\theta \approx 5^\circ$ does show good correspondence with a previously unexplained peak in the experimental diffraction pattern [Fig. 4(b)]. Thus, apart from decomposition into TiN and N_2, the formation of a semiconducting disordered defect rs phase of Ti_3N_4 is also a plausible product after decompression.

To summarize, we have synthesized c-Ti_3N_4 using diamond anvil cell experiments at 75 GPa. This phase exhibits the Th_3P_4-type structure with high cation and anion coordination numbers, which was previously observed for the group 4 counterparts, i.e., c-Zr_3N_4 and c-Hf_3N_4. Unlike the previous theoretical reports that predicted that c-Ti_3N_4 would be a narrow

band-gap semiconductor, the band gap of c-Ti_3N_4 estimated from our theoretical calculations is between 0.8 and 0.9 eV. The c-Ti_3N_4 phase is not recoverable below 5 GPa due to dynamic instabilities observed in phonon dispersion relations. We hypothesize that upon decompression, c-Ti_3N_4 could form a rs-derived disordered defect phase, which might transform into the predicted m-Ti_3N_4 phase upon ordering of Ti vacancies. Further experimental investigations towards this proposed metastable ambient pressure phase of Ti_3N_4 are warranted.

This work was supported by Energy Frontier Research in Extreme Environments (EFree) Center, an Energy Frontier Research Center (EFRC) funded by the U.S. Department of Energy, Office of Science under Award No. DE-SC0001057. S.L. was supported by the EFRC Center for Next Generation of Materials by Design (CNGMD). Portions of this work were performed at GeoSoilEnviroCARS (The University of Chicago, Sector 13IDD), Advanced Photon Source (APS), Argonne National Laboratory. GeoSoilEnviroCARS is supported by the National Science Foundation–Earth Sciences (EAR-1128799) and Department of Energy–GeoSciences (DE-FG02-94ER14466). A portion of this work was performed at HPCAT (Sector 16IDB), Advanced Photon Source (APS), Argonne National Laboratory. HPCAT operations are supported by DOE-NNSA under Award No. DE-NA0001974, with partial instrumentation funding by NSF. The Advanced Photon Source is a U.S. Department of Energy (DOE) Office of Science User Facility operated for the DOE Office of Science by Argonne National Laboratory under Contract No. DE-AC02-06CH11357.

[1] W. Lengauer, in *Handbook of Ceramic Hard Materials*, edited by R. Riedel (Wiley, New York, 2000), p. 202.
[2] H. O. Pierson, *Handbook of Refractory Carbides and Nitrides* (Noyes Publications, Westwood, NJ, 1996), p. 156.
[3] W. Spengler, R. Kaiser, A. N. Christensen, and G. Müller-Vogt, Phys. Rev. B **17**, 1095 (1978).
[4] T. D. Boyko, A. Hunt, A. Zerr, and A. Moewes, Phys. Rev. Lett. **111**, 097402 (2013).
[5] A. Zerr, G. Miehe, G. Serghiou, M. Schwarz, E. Kroke, R. Riedel, H. Fuesz, P. Kroll, and R. Boehler, Nature (London) **400**, 340 (1999).
[6] E. Horvath-Bordon, R. Riedel, A. Zerr, P. F. McMillan, G. Auffermann, Y. Prots, W. Bronger, R. Kniep, and P. Kroll, Chem. Soc. Rev. **35**, 987 (2006).
[7] A. Zerr, R. Riedel, T. Sekine, J. E. Lowther, W. Y. Ching, and I. Tanaka, Adv. Mater. **18**, 2933 (2006).
[8] A. Salamat, A. L. Hector, P. Kroll, and P. F. McMillan, Coord. Chem. Rev. **257**, 2063 (2013).
[9] W. Y. Ching, S.-D. Mo, L. Ouyang, I. Tanaka, and M. Yoshiya, Phys. Rev. B **61**, 10609 (2000).
[10] R. Juza and J. Heners, Z. Anorg. Allg. Chem. **332**, 159 (1964).
[11] M. Lerch, E. Füglein, and J. Wrba, Z. Anorg. Allg. Chem. **622**, 367 (1996).
[12] A. Zerr, G. Miehe, and R. Riedel, Nat. Mater. **2**, 185 (2003).
[13] P. Kroll, Phys. Rev. Lett. **90**, 125501 (2003).
[14] D. A. Dzivenko *et al.*, Adv. Mater. **19**, 1869 (2007).
[15] M. Chhowalla and H. E. Unalan, Nat. Mater. **4**, 317 (2005).
[16] M. Xu, S. Wang, G. Yin, J. Li, Y. Zheng, L. Chen, and Y. Jia, Appl. Phys. Lett. **89**, 151908 (2006).
[17] A. Kulkarni, J. C. Schön, K. Doll, and M. Jansen, Chem. - Asian J. **8**, 743 (2013).
[18] S. Yu, Q. Zeng, A. R. Oganov, G. Frapper, and L. Zhang, Phys. Chem. Chem. Phys. **17**, 11763 (2015).
[19] V. S. Bhadram, D. Y. Kim, and T. A. Strobel, Chem. Mater. **28**, 1616 (2016).
[20] W. Sun, A. Holder, B. Orvañanos, E. Arca, A. Zakutayev, S. Lany, and G. Ceder, Chem. Mater. **29**, 6936 (2017).
[21] W. Sun, S. T. Dacek, S. P. Ong, G. Hautier, A. Jain, W. D. Richards, A. C. Gamst, K. A. Persson, and G. Ceder, Sci. Adv. **2**, e1600225 (2016).
[22] A. Bikowski, S. Siol, J. Gu, A. Holder, J. S. Mangum, B. Gorman, W. Tumas, S. Lany, and A. Zakutayev, Chem. Mater. **29**, 6511 (2017).
[23] B. Anasori, M. R. Lukatskaya, and Y. Gogotsi, Nat. Rev. Mater. **2**, 16098 (2017).
[24] V. B. Prakapenka, A. Kubo, A. Kuznetsov, A. Laskin, O. Shkurikhin, P. Dera, M. L. Rivers, and S. R. Sutton, High Press. Res. **28**, 225 (2008).
[25] Y. Wang, J. Lv, L. Zhu, and Y. Ma, Phys. Rev. B **82**, 094116 (2010).
[26] Y. Wang, J. Lv, L. Zhu, and Y. Ma, Comput. Phys. Commun. **183**, 2063 (2012).
[27] J. P. Perdew, K. Burke, and M. Ernzerhof, Phys. Rev. Lett. **77**, 3865 (1996).
[28] A. V. Krukau, O. A. Vydrov, A. F. Izmaylov, and G. E. Scuseria, J. Chem. Phys. **125**, 224106 (2006).
[29] See Supplemental Material at http://link.aps.org/supplemental/10.1103/PhysRevMaterials.2.011602 for experimental and theoretical methods, additional XRD and Raman data, convex-hull diagram for Ti-N system with pressures, phonon dispersion relations of m-Ti_3N_4 (at 1 atm), c-Ti_3N_4 (at 70 GPa).
[30] A. Boultif and D. Louer, J. Appl. Crystallogr. **24**, 987 (1991).
[31] F. Holtzberg and S. Methfessel, J. Appl. Phys. **37**, 1433 (1966).
[32] P. L. Provenzano, S. I. Boldish, and W. B. White, Mater. Res. Bull. **12**, 939 (1977).
[33] P. S. Narayanan, Proc. Indian Acad. Sci. A **37**, 411 (1953).
[34] T. Ohsaka, F. Izumi, and Y. Fujiki, J. Raman Spectrosc. **7**, 321 (1978).
[35] G. Kresse and J. Furthmüller, Phys. Rev. B **54**, 11169 (1996).
[36] G. Kresse and D. Joubert, Phys. Rev. B **59**, 1758 (1999).
[37] C. M. Caskey, R. Richards, D. Ginley, and A. Zakutayev, Mater. Horiz. **1**, 424 (2014).
[38] K. Peter, J. Phys.: Condens. Matter **16**, S1235 (2004).
[39] A. Salamat, A. L. Hector, B. M. Gray, S. A. J. Kimber, P. Bouvier, and P. F. McMillan, J. Am. Chem. Soc. **135**, 9503 (2013).
[40] P. P. Zawadzki, J. Perkins, and S. Lany, Phys. Rev. B **90**, 094203 (2014).
[41] S. Lany, A. N. Fioretti, P. P. Zawadzki, L. T. Schelhas, E. S. Toberer, A. Zakutayev, and A. C. Tamboli, Phys. Rev. Mater. **1**, 035401 (2017).